

The University of San Francisco USF Scholarship: a digital repository @ Gleeson Library | Geschke Center

Master of Science in Analytics (MSAN) Faculty
Research

College of Arts and Sciences

7-10-2012

Laser Ablation-Inductively Coupled Plasma-Mass Spectrometry Analysis of Lower Pecos Rock Paints and Possible Pigment Sources

Jon Russ


Kaixuan Bu

Jeff Hamrick

University of San Francisco, jhamrick@usfca.edu

James V. Cizdziel

Follow this and additional works at: https://repository.usfca.edu/msan_fac

 Part of the [Analytical Chemistry Commons](#), and the [Archaeological Anthropology Commons](#)

Recommended Citation

Russ, Jon; Bu, Kaixuan; Hamrick, Jeff; and Cizdziel, James V., "Laser Ablation-Inductively Coupled Plasma-Mass Spectrometry Analysis of Lower Pecos Rock Paints and Possible Pigment Sources" (2012). *Master of Science in Analytics (MSAN) Faculty Research*. 5. https://repository.usfca.edu/msan_fac/5

This Article is brought to you for free and open access by the College of Arts and Sciences at USF Scholarship: a digital repository @ Gleeson Library | Geschke Center. It has been accepted for inclusion in Master of Science in Analytics (MSAN) Faculty Research by an authorized administrator of USF Scholarship: a digital repository @ Gleeson Library | Geschke Center. For more information, please contact repository@usfca.edu.

Laser Ablation-Inductively Coupled Plasma-Mass Spectrometry Analysis of Lower Pecos Rock Paints and Possible Pigment Sources

Jon Russ,^{1*} Kaixuan Bu,² Jeff Hamrick³ & James V. Cizdziel²

¹Department of Chemistry, Rhodes College, 2000 N. Parkway, Memphis, TN 3811, russj@rhodes.edu

²Department of Chemistry and Biochemistry, University of Mississippi, University, MS 38677

³Department of Mathematics and Computer Science, Rhodes College, 2000 N. Parkway, Memphis, TN 38112

Abstract

Chemical analyses of prehistoric rock paints from the Lower Pecos Region of southwestern Texas were undertaken using laser ablation-inductively coupled plasma-mass spectrometry. This technique allowed us to measure the chemical composition of the paint pigments with minimal interference from a natural rock coating that completely covers the ancient paints. We also analyzed samples representing potential sources of paint pigments, including iron-rich sandstones and quartzite from the study area and ten ochre samples from Arizona. Cluster analysis, principle component analysis and bivariate plots were used to compare the chemical compositions of the paint and pigment sources. The results indicate that limonite extracted from the sandstone was the most likely source for some of the pigments, while ochre was probably used as well.

Introduction

Studies of paleoart generally tend towards one of two strategies. The first can best be defined as iconography, in which motifs, themes, styles, placement, etc. are defined and used as comparison parameters. The second strategy is based on the physicochemical properties of the artifacts; in the case of pictographs, these properties usually include the chemical and mineral composition of the paints. Knowing the composition of the paint provides information on a variety of human activities and behaviors related to rock art production, such as how and where the paint materials were collected, how these substances were processed into paints, and the means by which the final product was applied to the rock surfaces. This can give direct evidence on the evolution and advancement of technologies used by prehistoric humans. Furthermore, the physicochemical characteristics of paints provide an independent means to compare and contrast assorted pictographs, one that is based on original paint recipes and not interpretations of the images (1).

We report here a study aimed at establishing the elemental composition of prehistoric rock paints from the Lower Pecos River region of southwestern Texas. Our objective was to determine whether there are chemical signatures in the paint that would allow us to identify the source(s) of the paint pigments and provide a means for comparing various pictographs. The Lower Pecos (Figure 1) contains one of the densest concentrations of rock art found anywhere, with more than 300 recognized rock art sites. The production of the rock art spans nearly 4000 years with the vast majority of the pictographs produced between 3000 and 4000 years ago. There were at least four different periods of pictograph production based on stylistic interpretations (2). Photographs and descriptions of the rock art can be found in a variety of publications (3,4,5).

A critical issue in analyzing ancient paints using current instrumental methods is that samples must be removed in order to perform most chemical analyses. Although there are a few techniques that can provide *in situ* analysis, for example portable X-Ray Fluorescence (XRF), most methods require samples to be brought into the laboratory. Bednarik (6) details the methods for collecting paint samples and the ethics of removing paint residues, mainly from the standpoint of direct dating of rock paints. Clearly, establishing the age of specific pictograms is important in terms of rock art studies, but developments and advances in analytical methods have emerged in the last several decades that allow paint chips or residues to be analyzed non-destructively, increasing the opportunity for multiple analyses to be performed in succession on a single sample (see for example, 7). The requirements of a “multi-technique” study is that each method be capable of analyzing very small samples with negligible (or no) loss of material and that the integrity of the sample remains post-analysis (i.e., it is not ground into a powder or chemically pretreated). Presently there are a variety of methods that satisfy these requirements including X-ray diffraction (XRD), Fourier-transform Raman Spectroscopy, Fourier-transform Infrared Spectroscopy (FTIR), particle induced X-ray emission (PIXE), optical microscopy, and microprobe microscopy, the latter in cases where the sample is not coated with a conductor. These techniques can be used in succession to provide distinct and overlapping information on the physicochemistry of the paints.

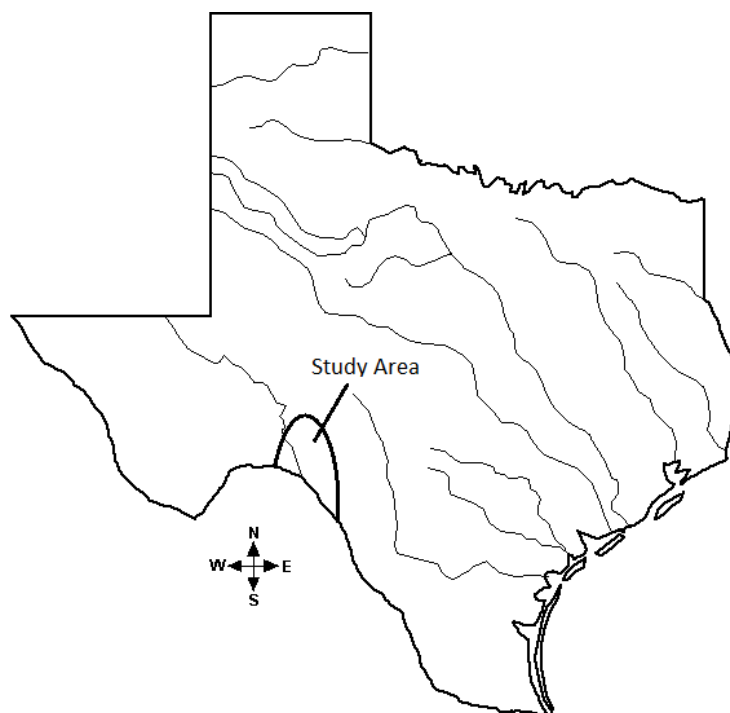


Figure 1. Map of Texas showing the approximate extent of the Lower Pecos Archaeological Region.

A relatively new method that fits the above criteria is laser ablation–inductively coupled plasma–mass spectrometry (LA-ICP-MS). This technique can be applied to very small samples (less than 1 mm of surface area) with negligible sample loss—usually less than 1.0 μg of sample is removed. Post-analysis the sample is essentially pristine. Moreover, the method yields accurate quantitative data for most elements, including trace elements at the parts-per-billion (ng g^{-1}) concentration range. LA-ICP-MS has become increasingly important in the study of archaeological materials (8,9,10) and has been used successfully for analyzing prehistoric rock paints located in Spain (11).

Of particular importance in employing LA-ICP-MS for the analysis of ancient rock paints is that elemental concentrations can be monitored in real-time as the laser ablates through the sample surface and into lower strata. Because most ancient paints are incorporated within or covered by natural rock coatings this facet of the output provides a distinct advantage of being able to identify when data from the paint layer is being acquired.

The physicochemistry of Lower Pecos rock paints

Lower Pecos pictographs have been studied extensively using scientific methods. The first analytical method applied to these artifacts was XRD by Zolensky in 1982 (12), where the mineral phases in the red, brown, orange and yellow pigments were determined to be iron-oxides, primarily Fe (II) and Fe (III) oxides, hydroxides, and hydrates (see also 13). Iron oxides were also consistently present in black paints but with inclusions of manganese oxide/hydroxide minerals, mainly pyrolusite and manganite.

Paint samples from the Lower Pecos Region were the primary materials used in the original proof-of-concept research that led to the development of the plasma-chemical extraction technique for ^{14}C dating rock paint (14,15). At least twenty-five individual Pecos River Style paint samples have since been radiocarbon dated using this technique, yielding data that demonstrated the viability of the plasma extraction method for isolating organic carbon for ^{14}C measurements. The results further established the period of production of the oldest and most extensive rock art style, the Pecos River Style, at between 3000- 4000 years ago (16). The production of these artifacts coincides with a time period when the human population in the region was at a local maximum (2).

The pigments used in Lower Pecos rock paints are demonstrably inorganic. But the mineral pigments do not produce a substance that can be used as a paint when simply added to water, especially not a paint that can yield thin, continuous, vibrant lines that are characteristic of many of the Pecos River Style motifs (Figure 2). The pigments must have suspended in a more viscous substance, probably an oily or greasy material that would serve as a suspender as well as a vehicle to bind the pigments to the rock substrate (3). The presence of such an organic material is the basis for the ^{14}C analysis of the rock art. That elevated concentrations of organic matter do occur in the Lower Pecos pictograph paints has been demonstrated through the low-temperature oxygen plasma extractions of organic (reduced) carbon in paint samples. Paint samples yielded considerably more CO_2 during the experiments as compared to extracts taken from rock surfaces collected next to the painting (15).

The nature and source of the organic material used in Lower Pecos paints remains a mystery. It is generally assumed that animal fats or plant juices were used to prepare the paints. Reese et al. (17) attempted to identify the source of the organics using DNA extracted from the paints and amplified using PCR. This work initially indicated that there was animal DNA in the paint; however, these experiments were not reproducible (18). Extractions of lipids (focusing on bound and unbound fatty acids) from the ancient paints were also performed and analyzed using GC-MS (19). The results showed that the paint samples and non-painted surfaces next to paints have the same fatty acid compositions and concentrations. It stands to reason that these detected organic compounds were not those deliberately added to the paints, but instead the product of the organisms that grow naturally on the rock surfaces (which we address below). It is likely that any organic matter that was added to the paint mixture has polymerized over the past three to four millennia, and is no longer in the original molecular form.

All the extant rock paintings in the Lower Pecos region occur in dry rock shelters and under rock overhangs. The limestone surfaces in these environments, i.e., surfaces protected from rain and runoff, are completely covered with a natural rock coating composed almost entirely of calcium oxalate (20,21). The

pictograph paints are encapsulated within this oxalate-rich coating (Figure 3). Oxalate-rich rock coatings are common under rock overhangs world-wide, and occur on surfaces that also contain rock art in Australia (22), Africa (23), Spain (24) and Brazil (25).



Figure 2. Photograph of a Pecos Style pictograph (~ 1 m tall) where very fine lines of red and black paint were used to produce what appear to be wings, red paint that outlines the body, and individual toes. This suggests that some form of an organic substance was used to suspend the inorganic pigments.

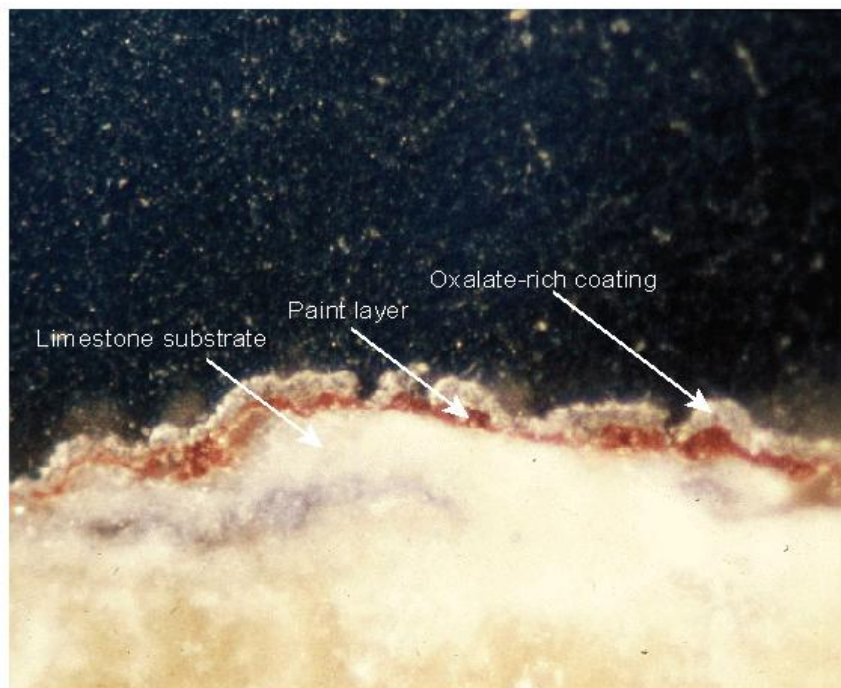


Figure 3. Optical photograph of a thin-sectioned paint sample showing the stratigraphy of the oxalate-rich coating, the paint layer, and the basal limestone.

The natural rock coating that occurs in Lower Pecos rock shelters is generally ~500 µm thick with micro-intrusions of gypsum from efflorescence and clay deposits, both of which occur on the surface and imbedded within the coating as observed using SEM-EDS (26, 27). There were also microstructures observed in the coating that resembled features observed in lichens (27), which are known to produce calcium oxalates. Hess et al. (28), however, demonstrated that at least five species of oxalate-producing bacteria (mainly *Bacillus*) occur on or within the rock coating. Whether produced by lichen and/or bacteria, the oxalate is definitely biogenic and radiocarbon analyses of the coating indicate it was produced episodically during the middle and late Holocene (29).

The SEM analysis of paint samples showed that the paint layers were generally ~100 µm thick and discontinuous. In all cases the paint layers were completely covered by the oxalate coating and usually at the interface between the basal limestone and coating (20).

In summary, we can state unambiguously that the Lower Pecos rock paints were prepared primarily from iron oxides between 3000-4000 years ago and that these pigments are currently encapsulated within a naturally occurring, 500 µm thick rock coating. The coating is mainly calcium oxalate with minor amounts of gypsum and clays incorporated within and on the surfaces of the coating.

Possible sources of pigments

Source(s) of Lower Pecos paint pigments have been speculated on for many decades. For example, Kirkland noted as far back as 1934 that a variety of local materials could have been used for Pecos River pigments including “limonite” (a native iron-rich sandstone) as well as other brown, red and orange stones common in the dry creek beds (3). The limonite pebbles are softer and easier to work with compared to the harder but more iron rich quartzite stones. The iron content of the limonite sandstones is much too low to be used directly as a pigment, and so it would have been necessary to extract the iron-rich component from the sandstone. Ochre was also suggested as a possible pigment, a material that would not necessarily require preprocessing (3).

Turpin reported on two large pigment cakes, each weighing ~ 1 kg, that had been excavated from two Lower Pecos rock shelters (30). The nature of the cakes made it clear that if these were precursors to pictograph paints then some form of pre-processing of the pigments was used. Turpin (30) further noted that the most likely source of the pigment cakes were the local limonite stones, but that significant enrichment of the iron was necessary. She suggested that a similar technique, described by Lorblanchet et al. (31), for the production of Paleolithic paints in Europe was used by the Lower Pecos people to construct the pigment cakes. The extraction of the iron component involved grinding the pebbles and then putting the powder in water. The sandstone quartz would settle out and the iron-containing component would be suspended in the water to be isolated. The color of the material could be manipulated and enhanced by heating the iron extract to remove hydrates from the mineral matrix, creating different shades of red, yellow, orange and brown.

Another potential source of iron for the paint pigments could have been iron-rich quartzite stones, also common in dry creek beds in the region. Compared to the friable limonite sandstones the quartzite is considerably harder and much more difficult to grind into a powder, a process that would be necessary to produce the pigments.

Methods

Samples

We analyzed five different types of samples for this study: (a) Prehistoric paint chips from four sites in the Lower Pecos Region, (b) ochre from three sites in Arizona, (c) iron-rich sandstone (limonite) pebbles collected from dry creek beds in the Lower Pecos, (d) an iron-rich quartzite stone, and (e) samples of the oxalate-rich rock coating collected from non-painted surfaces in the rock shelters.

- (a) Prehistoric paints: Sixteen red paint samples from four different rock art sites were analyzed for this study. We obtained nine paint samples from five different areas inside site 41VV75. Most of the paints in the sampled surfaces appear to have merged into one amorphous montage, and so the individual pictographs could not be differentiated. We also analyzed six samples from 41VV576 collected from two different areas of what appeared to be the same pictograph. Two additional samples, one each from sites 41VV124 and 41VV127, were included in the study. All the paint samples were most likely from Pecos River Style paintings, and thus produced between 3000-4000 years ago.
- (b) Ochre: Ten ochre samples originally collected and analyzed using Instrumental Neutron Activation Analysis (INAA) by Popelka-Filcoff et al. (32), were included in this study. The samples were collected from three different geological formations in southern Arizona (Beehive Peak, Ragged Top and Rattlesnake Pass). The elemental signatures in the ochre were determined to be site specific, thus demonstrating that elemental fingerprinting could be used for provenance studies of these ochre formations. For our analysis we prepared the samples by grinding them using an agate mortar and pestle and then pressing them into pellets using a pellet press under 12,000 psi for five minutes. We analyzed the pellets using XRF prior to the LA-ICP-MS analysis.
- (c) Iron-rich (limonite) sandstones: We prepared three samples from sandstone (limonite) pebbles collected from dry creek beds in the Lower Pecos region. The Munsell color of the original stones ranged from 10YR8/3 to 2.5YR6/6 and with a hardness of ~2 on the Mohs scale. The samples were prepared by emulating the method described by Lorblanchet et al. (31), which involved grinding the pebbles in an agate mortar and pestle and placing the powder in a beaker with deionized water. The heavier quartz was allowed to settle to the beaker bottom; then, the liquid phase with the limonite component decanted. The liquid was transferred to a watchglass and the water evaporated in a 100°C oven. The resulting powder was heated over a Bunsen burner for several hours to increase the redness, and then pressed into pellets as described above. The color of the pellets were significantly darker and redder (colors ranging from 5YR6/6 to 10R6/6) when compared to the original limonite pebbles. Moreover, the iron concentration increased from < 1% Fe in the pebbles to an average of 2.3% Fe in the pellets, as measured using XRF.
- (d) Iron-rich quartzite: There are a variety of different colored rocks in the dry creek beds throughout the study area, some potentially used as pigments (3). One that matches closely with the pigment color is a dark red quartzite with a Munsell color of 10R2.5/2. The iron content of the quartzite stone we analyzed was 3.4 % Fe and with a Mohs hardness of ~ 7. Chips of this stone were analyzed directly.
- (e) Oxalate coating: Since all paints are incorporated within the natural oxalate-rich rock coating we analyzed six individual samples collected from inside two of the rock shelters (41VV75 and 41VV576). We had five samples from site 41VV75 and one from sample site 41VV576; however, no samples from the other two sites (41VV224 and 41VV227) were available

LA-ICP-MS Instrumentation, data acquisition and data reduction

The ICP-MS used was an X-Series 2 (Thermo-Fisher Scientific, Waltham, MA, USA). The instrument employs a quadrupole mass analyzer (filter) which provides fast scanning capability required for transient signals. Laser ablation was conducted using a UP-213 system (New Wave Research, Fremont, CA, USA). The UP-213 employs a frequency quintupled Nd:YAG laser with a resulting wavelength of 213 nm. Helium (0.8 L min⁻¹) was used as the cell carrier gas; argon (0.7 L min⁻¹) was added prior to entering the plasma. The LA-ICP-MS system was optimized for sensitivity and oxides prior to analysis using NIST glass reference materials (SRM 612). The instrumental settings for the LA-ICPMS analyses are summarized in Table 1. Briefly, the UP-213 was operated at 40% power, with a repetition rate of 2 Hz, and a spot size of 100 μm. Data was collected while performing spot shots at the surface of the rock samples. Each ablation lasted for about 3 minutes, including 20 seconds before the laser was fired to collect background levels (gas blank) and 60 seconds for preceding signal tail wash out. The ICP-MS was operated in peak jump mode. Raw elemental intensities were processed using the X-Series software, where the data was reduced and concentrations were determined. Calcium was used as the internal standard, except for the paint layer where Fe was used (see XRF section below). For quantification, we used a microanalytical carbonate standard (MACS-3) prepared by the USGS using a co-precipitation process in which trace and minor elements were mixed with the precipitate. A second carbonate material (GP-4, also from the USGS) was used for quality assurance purposes. The GP-4 material was used in a proficiency testing program for microanalytical work. Both materials are available in pressed pellet form.

Table 1. LA-ICPMS instrument settings.

UP-213 system	
Laser type	Nd-YAG
Wavelength	213 nm
Power	40 %
Frequency	2 Hz
Carrier gas	He
Carrier gas flow	0.8 L min ⁻¹
Scan type	Spot
Spot size	100 μm
Duration per scan	~3 min
Plasma	
Cool gas flow	13.5 L min ⁻¹
Aux. gas flow	0.6 L min ⁻¹
Sample gas flow (Ar)	0.7 L min ⁻¹
Resolution	125
Data Acquisition	
Isotopes monitored	²⁴ Mg, ⁴⁴ Ca, ⁵¹ V, ⁵³ Cr, ⁵⁵ Mn, ⁵⁷ Fe, ⁵⁹ Co, ⁶⁶ Zn, ⁷⁵ As, ⁸² Se, ⁹⁰ Zr, ⁹⁵ Mo, ¹¹⁵ In, ¹²¹ Sb, ¹³⁹ La, ¹⁴⁶ Nd, ¹⁵³ Eu, ¹⁷⁵ Lu
Integration time	10 ms

The relatively low laser power/frequency settings were selected to facilitate discrimination between the coating, paint and substrate during the ablation process, and to optimize the iron signal. This can be seen in Figure 4, where line scans represent the relative concentration of three elements: Ca, Fe and Mg. As the laser ablates through the rock coating, the Ca signal remains relatively level due to the dominate material being calcium oxalate. As the ablation proceeds into the paint layer, the Fe concentration increases dramatically due to the high concentration of iron oxides. Finally, as the laser penetrates through the paint it begins to interact with the limestone substrate, which contains relatively high Mg concentration, which is observed by the simultaneous decrease in Fe and increase in Mg. To determine the concentration of the elements of interest the signal from these elements were integrated over the area where the iron peak was observed.

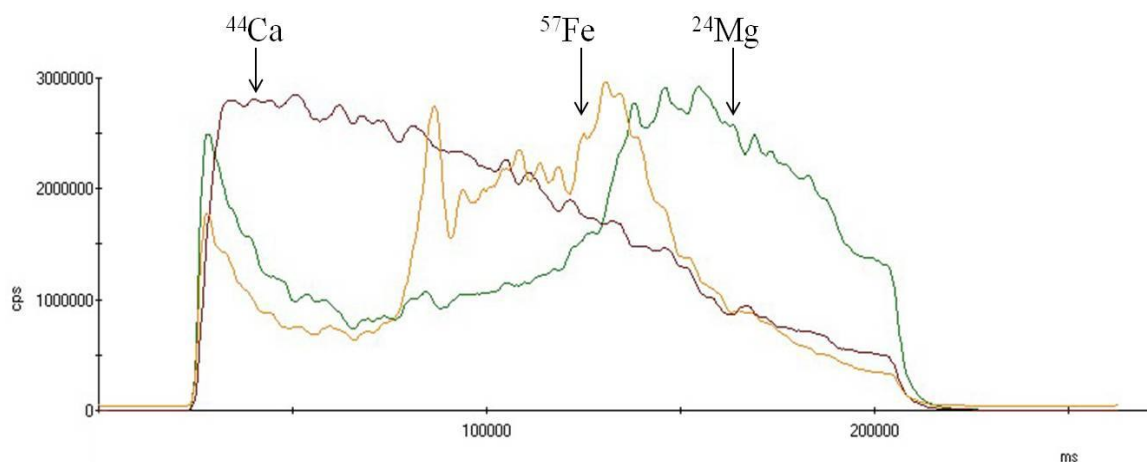


Figure 4. Typical elemental intensity variation during laser depth profiling. The rise in ^{57}Fe indicates ablation has reached a paint layer, and the rise in ^{24}Mg indicates the ablation has reached the limestone substrate layer.

We initially measured the concentrations of 37 elements in one red paint sample (75RP-34) and one coating sample (75-31) to determine which elements correlated with the Fe concentration using Pearson's correlation coefficients. Of the 36 elements, ten correlated positively with Fe ($r > 0.9$) in the paint sample (V, Cr, As, Zr, Mo, In, Sb, La, and Nd), whereas only Cr correlated with Fe in the coating. We selected the above elements for our analyses in subsequent measurements.

XRF

We analyzed the ochre, iron-rich quartzite, limonite pellets, and unmodified limonite pebbles using an Innove-X α -4000 AS X-Ray Fluorescence (XRF) spectrometer. Because the ablation process can result in varying amounts of sample reaching the plasma, an internal standard is used to compensate for fluctuating signals stemming from this mass transport process. For the paint layer, we used Fe as the internal standard; elemental signals measured by LA-ICP-MS were normalized to the Fe signal. The Fe concentration determined from the XRF analysis was used for quantification.

Results

Concentrations of the ten elements (V, Cr, Fe, As, Zr, Mo, In, Sb, La, and Nd) were measured in six rock coating samples, sixteen red paint samples, ten ocher samples, three limonite samples, and one quartzite sample using LA-ICP-MS (Appendix 1). All detectable elements from the XRF analysis are given in Appendix 2.

Chemistry of the coating and ancient paints

A primary issue for obtaining reliable data from the paint analysis was the presence of each element of interest in the crust, i.e., the background. This was especially true for iron since it was the dominant element in the paint and the basis for the color. The iron concentrations of the rock coatings from site 41VV75 (5 samples) ranged from 0.0373% to 0.254% with an average of $0.13 \pm 0.10\%$. The average iron concentration in the eight red paint samples from site 41VV75 was $4.3 \pm 2.1\%$; therefore, on average, the coatings contribute 2.9% Fe (Table 2). At site 41VV576, the iron concentration in the one coating sample measured $0.82 \pm 0.34\%$ Fe, a value that is four times greater than the coating concentration at 41VV75.

The six paint samples from site 41VV576 contained $8.2 \pm 7.8\%$ Fe, and thus ten times greater than the average iron content of the coating from this site. The sample from site 41VV227 was $2.46 \pm 0.19\%$ Fe based on four repeat analyses of the one sample. Only one spot analysis of the single sample from site 41VV224 (out of four attempted) had a measured iron concentration significantly higher than the coatings from 41VV75 or 41VV576, a value of 2.6 % Fe, and so we used only this result.

Of the other eight elements included in the analyses, V, As, Mo and Sb had the lowest relative percentage in the crust compared to the paint, whereas, Cr, Zr, La and Nd had the highest relative percentages. Therefore, the former elements should more reliable in representing the composition of the paints, since they have the least relative contribution from the coating.

Table 2. Average concentration of the elements of interest in the coating and paint samples collected from two sites in the Lower Pecos (sites 41VV75 and 41VV576). Also shown are the relative proportions (%) of each element in the coating compared to the paint.

Element	Site 41VV75			Site 41VV576		
	Coating (ppm)	Paint (ppm)	Relative % coating/paint	Coating (ppm)	Paint (ppm)	Relative % coating/paint
V	15.6	274	5.7	51.9	961	5.4
Cr	5.07	22.4	22.6	10.4	11.4	91.4
Fe	1252	42530	2.9	8200	77750	10.5
As	10.4	121	8.5	26.5	245	10.8
Zr	5.27	36.9	14.3	19.0	19.4	98.0
Mo	3.30	85.4	3.9	4.36	43.7	10.0
Sb	0.34	7.07	4.8	0.39	6.95	5.6
La	2.44	18.8	13.0	4.70	4.77	98.5
Nd	2.21	19.4	11.4	4.70	5.41	86.9

Hierarchical cluster analysis

Ward's method of cluster analysis was used to draw conclusions about the similarities of the total chemical composition of the samples of paint, ochre, sandstone, and iron-rich quartzite (Figure 5). Ward's method minimizes the total within-cluster variance in the data, i.e., at each step, the pair of cluster with the minimum cluster distance is merged. The usefulness of this approach is revealed in the clustering of the ochre data. These samples originated from three different locations. Ward's method consistently placed the five samples from the Beehive formation (BH), the four samples from the Rattlesnake Pass (RP), and the one sample from Ragged Top (RT) in independent clusters. The dendrogram also shows that the iron-rich quartzite collected from the Lower Pecos is chemically more similar to the ochre than the paints or limonite sandstone, and that the ochre and the quartzite are distinct from the latter.

The three extracted limonite samples form an independent cluster that is more closely related to the paints than the ochre or quartzite. Moreover, one paint sample from site 41VV576 is more closely related chemically to the limonite than the other paint samples in this study.

The cluster analysis further reveals that the paint composition from samples collected from different sites are often more similar as compared to paints collected from the same site. There is only one first order cluster consisting of paints from the sites (three samples from 41VV576), and one second order cluster also with three samples from a single site (41VV75), but the remainder of the first and second order clusters contain samples from a multiple sites.

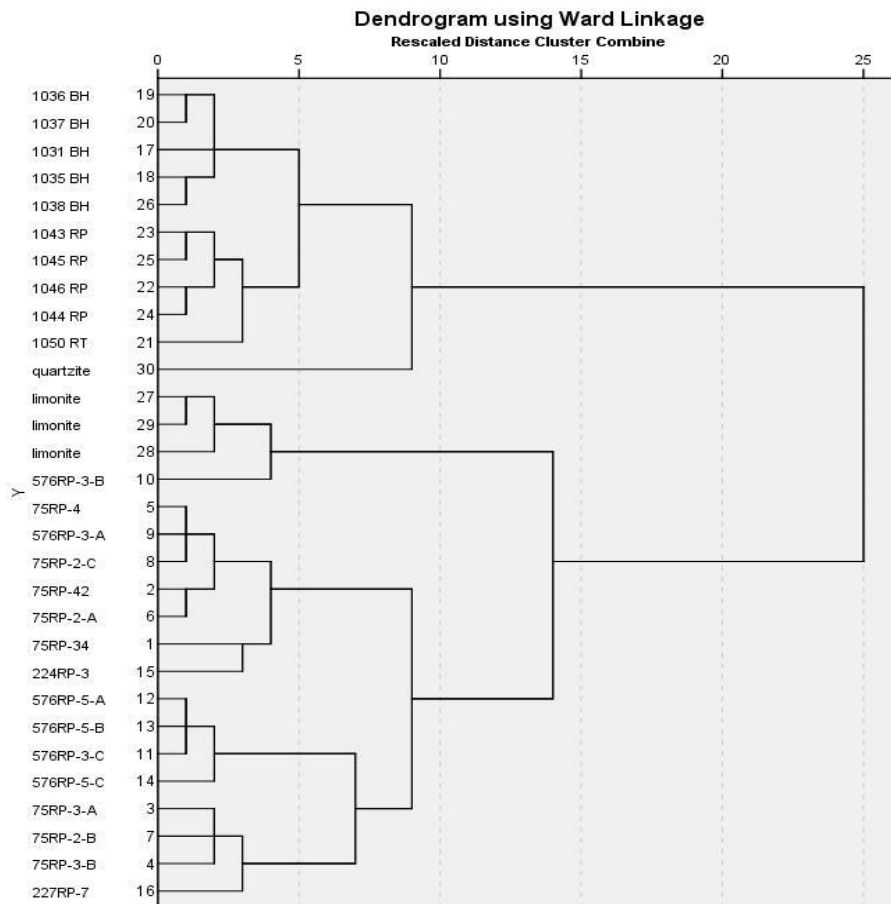


Figure 5. Dendrogram showing the hierarchical clustering based on Wards Method using the total chemical composition of the paints, sandstone (limonite), ochre and iron-rich quartzite (iron-nodule).

Principle component analysis (PCA)

Additional comparisons between the paints and potential pigment sources were explored using PCA to determine which elements in our data set contributed most significantly to the variance in the data (Figure 6). From the plot, we ascertained that two principal components characterize approximately 75% of the variation in the elemental data. PCA 1 is the dominant component, which is consistent in that most of the scored data variation lies along the x-axis (assigned to PCA 1). The vectors indicate which chemical elements are responsible for most of PCA 1; namely, the vectors most parallel to the x-axis. Hence PCA 1 is mostly driven by the presence (or lack thereof) of Mo, La, Nd, and Zr. These elements make little, if any, contribution to PCA 2.

PCA 2 is a much weaker factor, as indicated on this plot by the fact that few of the chemical elements are strongly parallel to the y-axis. However, most of the information driving PCA 2 is provided by V, As, Sb, and Cr. Recall that vectors that are nearly parallel are redundant for purposes of the classification (for example, La, Nd, and Zr are highly correlated in the samples and they basically tell the same story about those samples). The elements Sb and Cr, similarly, provide nearly identical information, while V and As are the most interesting for purposes of adding new information to the analysis since they provide very different information than Sb and Cr.

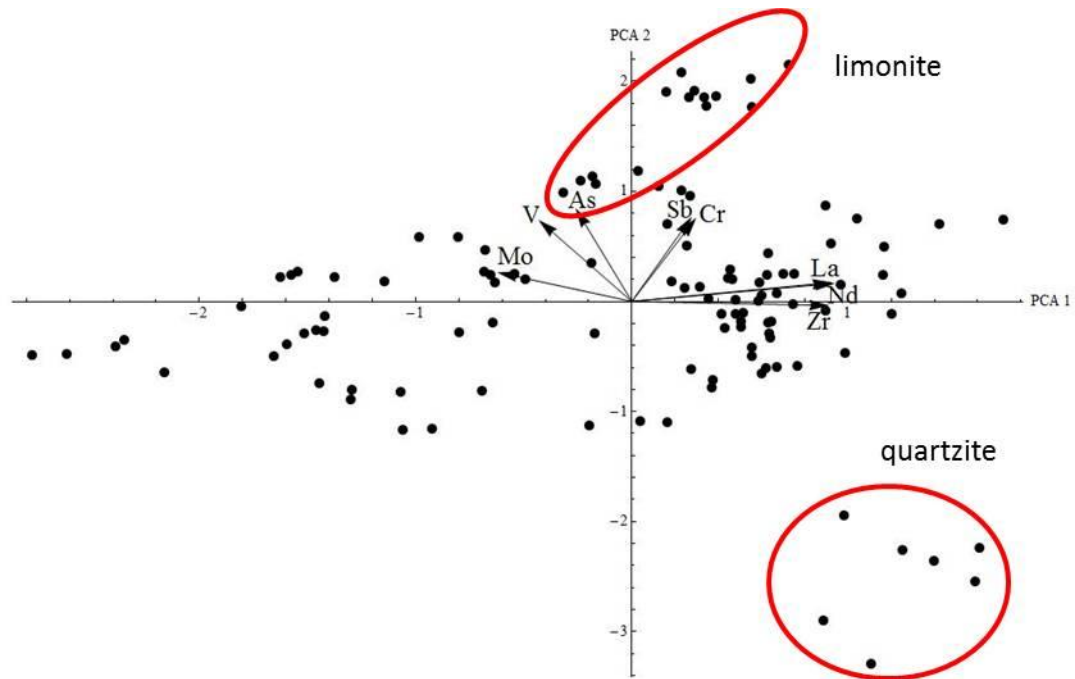


Figure 6. Principle component analysis (PCA) of PC 1 versus PC 2 showing which elements contribute most of the variance in the data, as expressed by the total chemical composition of the samples.

Bivariate plots

Based on the PCA we concluded that the elemental concentrations driving the variance in the data, and thus the most useful in associating the paints with particular pigment sources, were V, As, Sb and Cr. However, because Cr has a relatively high concentration in the coating compared to the paint we eliminated this element due to the expected interference.

The two bivariate plots below demonstrate that the three potential sources of pigments are distinguishable based on the V, As and Sb concentrations (Figures 7 and 8). From these plots it is apparent that the paints are least similar to the iron-rich quartzite. In both graphs the paint data generally fall between the ochre and sandstone data. The As - V plot shows that there considerable overlap with the ochre and paint samples from 41VV75, and the paints from 41VV576 are more closely associated with the limonite in this plot (Figure 8).

Comparisons between the paint samples show that there is a chemical distinction between the V, As, and Sb content in samples from 41VV576 and 41VV75. The one paint sample from 31VV227 is chemically the same as those from 41VV576, while the single paint from 41VV224 is more closely related to the samples from 41VV75.

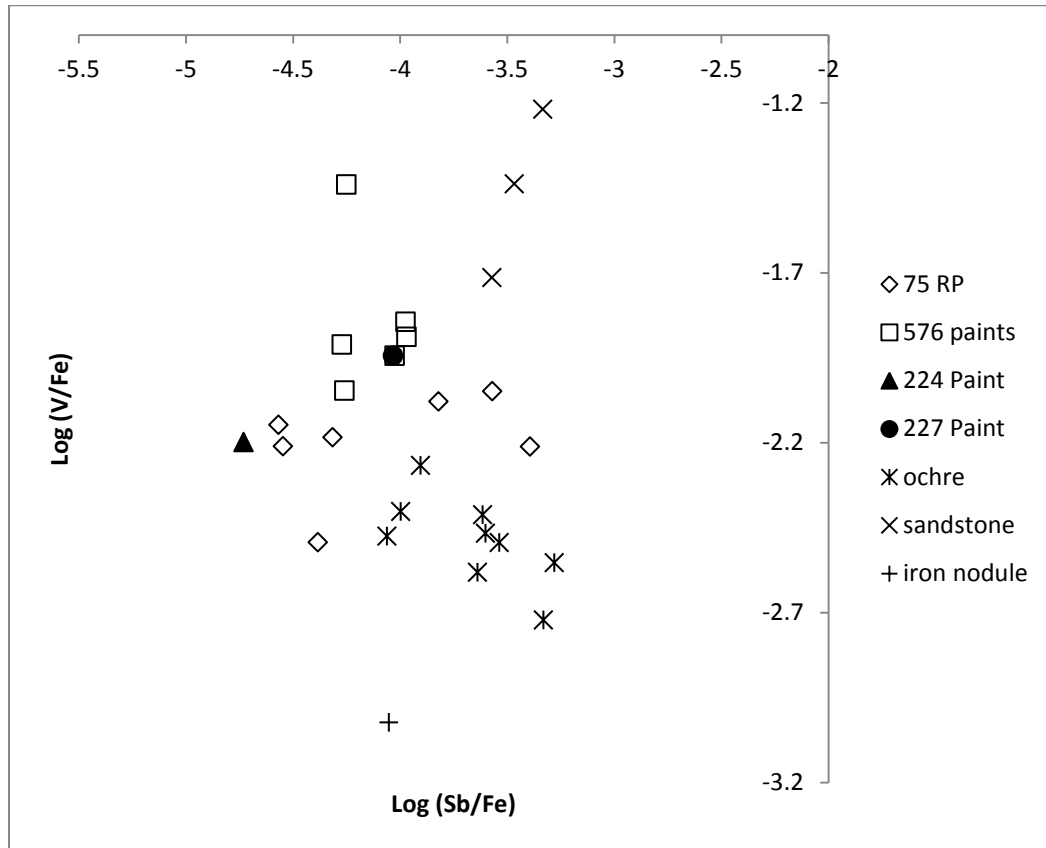


Figure 7. $\text{Log}_{10}(\text{Sb}/\text{Fe})$ versus $\text{Log}_{10}(\text{V}/\text{Fe})$ bivariate plot showing two dimensional relationships between the samples.

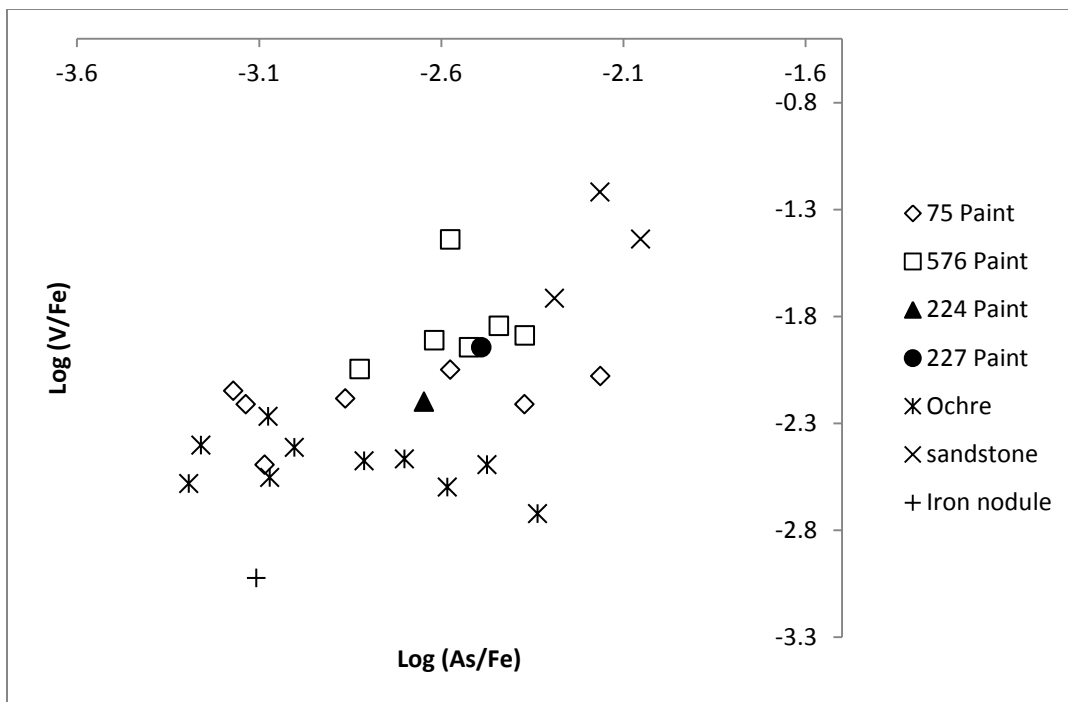


Figure 8. $\text{Log}_{10}(\text{As}/\text{Fe})$ versus $\text{Log}_{10}(\text{V}/\text{Fe})$ bivariate plot showing two dimensional relationships between the samples.

Discussion

LA-ICP-MS proved to be a useful technique for obtaining elemental data from samples containing prehistoric rock paints. The samples we studied remained essentially pristine post-analysis, with negligible amount of paint material removed and with no adverse effects to the sample integrity.

The application of the Ward's Method and bivariate plots consistently supported the hypothesis by Turpin (2) that the local iron-rich sandstones (limonite) was at least one source of the Lower Pecos paint pigments. This further indicates that the people that produced the paints were technologically advance enough to isolate the limonite from the sandstone and manipulate the color by dehydrating the iron (31). On the other hand, the local quartzite stone, despite having a much higher iron content than the sandstone and a native color similar to many of the paints, was not used in the production of the paints we studied. Finally, the chemical similarities between some of the paints and ochre samples from Arizona suggest that an analogous source was used in paint production.

Acknowledgements

The ICPMS used in this study was obtained through a NSF grant (Award #0923080). We thank Tristan Hill, Sydney Milton, Jaala Spencer for assistance with preliminary LA-ICP-MS analysis; David Jeter for help with the XRF analysis; and Chris Mouron for assistance with preliminary statistics. Part of this research was funded by a Rhodes Faculty Development Grant.

References

1. Menu, M.; Walter, P.; *Nucl. Instrum. Methods.* **1992**, *B64*, 547-552.
2. Turpin, S. A.; *American Indian Rock Art*; Proceedings of the International Rock Art Conference: San Antonio, TX, 1990 Vol. 16, pp 99-122.
3. Kirkland, F.; Newcomb, W. W. *The Rock Art of Texas Indians*; The University of Texas Press: Austin, TX, 1967, pp 239.
4. Shafer, H. J.; Zintgraph, J.; *Ancient Texans: Rock Art and Lifeways Along the Lower Pecos*; San Antonio Museum Association: San Antonio, TX, 1986, pp 247.
5. Boyd, C. E.; *Rock Art of the Lower Pecos*; Texas A&M University Press: College Station, TX, 2003, pp. 153.
6. Bednarik, R. G.; *Rock Art Science: The Scientific Study of Paleoart*; New Delhi, India, 2007, pp 174-175.
7. Bonneau, A.; Pearce, D. G.; Pollard, A. M.; *J. Archaeol. Sci.* **2012**, *39*, 287-294.
8. Speakman, R. J.; Neff, H.; In *Laser Ablation-ICP-MS in Archaeological Research*; Editors: R. J. Speakman and H. Neff, University of New Mexico, Albuquerque, NM, 2005, pp 1-14.
9. Guiassani, B.; Monticelli, D.; Rampazzi, L.; *Anal. Chim. Acta.* **2009**, *635*, 6-21.
10. Resano, M.; Garcia-Ruiz, E.; Vanhaecke, F.; *Mass Spectrom. Rev.* **2010**, *29*, 55-78.
11. Resano, M.; Garcia-Ruiz, E.; Alloza, R.; Marzo, M. P.; Vandenabeele, P.; Vanhaecke, F.; *Anal. Chem.* **2007**, *79*, 8947-8955.
12. Zolensky, M.; In *Seminole Canyon: The Art and the Archeology. Texas Archeological Survey Research Report No. 83.* The University of Texas Press, Austin, TX pp 277-284.
13. Hyman, M.; Turpin, S. A.; Zolensky, M. E.; *Rock Art Res.* **1996**, *13*, 93-103.
14. Russ, J.; Hyman, M.; Shafer, H. J.; Rowe, M. W. *Nature* **1990**, *348*, 710-711.
15. Ilger, W.; Hyman, M.; Southon, J., Rowe, M. W. *Radiocarbon* **1995**, *37*, 299-310.
16. Rowe, M. W., *Anal. Chem.* **2009**, *81*, 1728-1735.
17. Reese, R.; Hyman, M.; Rowe, M. W.; Derr, J. N.; Davis, S. K.; *J. Archaeol. Sci.* **1996**, *23*, 269-277.
18. Mawk, E. J.; Hyman, M.; Rowe, M. W.; *J. Archaeol. Sci.* **2002**, *29*, 301-306.
19. Spades, S.; Russ, J.; *Archaeometry* **2005**, *47*, 115-126.
20. Russ, J.; Kaluarachchi, W. D.; Drummon, L.; Edwards, H. G. M.; *Stud. Conserv.* **1999**, *44*, 91-103.
21. Russ, J.; Palma, R. L.; Loyd, D. H.; Farwell, D. W.; Edwards, H. G. M.; *Geoarchaeology* **1995**, *10*, 43-63
22. Watchman, A.; *Rock Art Res.* **1990**, *7*, 44-50.
23. Mazel, A. D.; Watchman, A. L. *South. Afr. Humanit.* **2003**, *15*, 59-73.
24. Hernanz, A.; Gavira-Vallejo, J. M.; Ruiz-Lopez, J. F.; Edwards, H. G. M.; *J. Raman Spectrosc.* 2008, *39*, 972-984.
25. Steelman, K. L.; Rickman, R.; Rowe, M. W.; Boutton, T. W.; Russ, J.; Guidon, N.; In *Archaeological Chemistry ACS Symposium*; Editor, K. A. Jakes; Series 831: American Chemical Society, Washington, DC. 2002, pp 22-35.
26. Kaluarachchi, W.; M.S. thesis, Sam Houston State University, Huntsville, TX, 1995.
27. Russ, J.; R. L. Palma, D. H.; Loyd, T. W.; Boutton T. W.; Coy, M. A. *Quaternary Res.* **1996**, *46*, 27-36.

28. Hess, D.; Coker, D. J.; Loutsch, J. M.; Russ, J.; *Geoarchaeology* **2008**, 23, 3-11.
29. Russ, J.; Loyd, D.; Boutton, T. W.; *Quatern. Int.* **2000**, 67, 29-36.
30. Turpin, S. A.; *J. Southern. Tex. Arch. Soc.* **1997**, 24, 34-37.
31. Lorblanchet, M.; Labeau, M.; Vernet, J.-L.; Fitte, P.; Valladas, H.; Cachier, H.; Arnold, M.; *Rock Art Res.* **1990**, 7, 4-20.
32. Popelka-Filcoff, R.S.; Miksa, E. J.; Roberston, J. D.; Glascock, M. D.; Wallace, H.; *J. Archaeol. Sci.* **2008**, 35, 752-762.

Appendix 1. Elemental concentrations (ppm) of rock coatings, ochre, prehistoric paints, limonite, and an iron-rich quartzite (nodule).

Sample type	Sample Number	Elemental concentrations (ppm)									
		V	Cr	Fe	As	Zr	Mo	In	Sb	La	Nd
<i>Rock Coatings</i>											
	75C-31	25.37	0.562	866.7	16.28	2.018	13.34	0	0.049	1.624	1.462
		16.16	0.458	595.9	19.74	0.714	2.214	0	0.052	1.925	1.817
		22.51	0.374	500.3	-1.89	2.142	6.877	0	0.011	1.796	1.22
	75C-1-A	24.34	8.866	2890	22.74	30.81	2.714	0.004	1.864	6.006	6.427
		16.33	6.668	1300	17.7	3.076	2.018	0	0.315	2.656	2.235
		7.827	5.403	397	8.853	1.619	1.062	0	0.162	1.453	1.271
	75C-1-B	17.06	7.731	1845	17.57	8.39	2.474	0	0.465	3.463	3.217
		12.8	4.59	1038	10.75	3.382	3.005	0	0.436	1.897	1.704
		17.2	6.334	689.5	10.3	2.142	1.175	0.002	0.237	1.462	1.122
	75C-1-C	19.18	9.39	1469	7.488	3.915	2.221	0	0.463	1.824	1.585
		17.41	8.895	2762	6.683	8.751	2.77	0.001	0.418	4.459	4.389
		21.52	9.48	3312	6.204	9.291	2.514	0.004	0.463	3.493	3.469
	75C-1-D	6.323	2.858	293.4	12.32	0.761	0.278	0	0.03	1.894	1.611
		2.763	0.787	173.9	10.86	0.288	2.499	0	0.024	0.863	0.369
		7.361	3.692	653.3	11.67	1.706	4.266	0.03	0.143	1.837	1.26
	576C-1-A	56.59	11.41	7829	28.07	16.77	5.634	0	0.711	5.048	5.572
		32.25	8.38	5042	15.3	9.893	2.577	0.003	0.168	4.578	4.324
		66.7	11.4	11720	36.22	30.3	4.88	0.059	0.29	4.462	4.209
<i>Red Paints</i>											
	75RP-34	167	1.904	26020	21.18	15.11	14.73	0	0.662	5.821	6.185
		85.94	1.257	14240	8.013	166	11.11	0	0.509	5.355	4.63
		130.3	1.839	22010	16.29	16.5	13.36	0	0.596	5.529	5.996
	75RP-42	178.3	91.48	72570	52.48	22.83	161.2	0.014	2.008	16.54	17.22
		194.6	105.2	49160	53.61	46.63	172.2	0.03	2.545	20.21	20.08
		94.38	43.45	23780	13.88	22.02	51.82	0	1.462	19.87	24.45
	75RP-3-A*	230.9	11.9	25640	68.92	10.95	128.5	0.004	7.183	9.574	10.64
		59.7	10.86	9890	22.71	11.25	26.41	0.006	1.804	7.909	8.016
		174.1	12.41	19680	51.84	15.23	82.52	0.004	5.012	8.18	7.882
	75RP-3-B*	326.9	9.868	58860	248.1	39.82	58.2	0.007	22.99	4.374	5.398
		638.6	12.7	103800	430.4	24.5	102.7	0.005	42.53	8.127	9.117
		604	12.05	92770	409.2	24.99	86.52	0	37.71	8.806	8.538
	75RP-4	198.2	16.26	29880	45.48	29.61	39.3	0.013	1.629	9.079	9.125
		473.9	18.63	73990	67.26	25.74	110.3	0.012	3.022	9.611	9.667
		97.4	15.72	13800	48.59	23.66	22.96	0.012	1.039	12.89	14.16
	75RP-2-A*	385.9	43.62	53310	23.3	18.02	73.66	0.011	1.153	7.629	9.765
		237.1	3.156	34230	35.79	38.25	44.19	0.006	1.215	15.6	16.38
	75RP-2-B*	487.6	9.871	44150	158.2	73.29	113.9	0	5.147	21.62	20.49
		359	23.05	57380	728.8	117.9	149.4	0	11.9	177.3	179
		321.2	23.87	38550	75.85	40.39	80.68	0.029	4.128	24.71	25.01
	75RP-2-C*	159.4	13.22	21070	63.76	24.01	73.17	0.046	1.39	12.56	12.55

	157.4	17.78	21310	51.67	20.21	79.28	0.003	1.849	11.79	11.87
	529.1	15.51	72040	97.48	22.93	268.7	0.023	5.046	9.603	8.869
576RP-3-A*	407.7	7.517	35940	67.17	11.71	36.67	0.002	2.283	4.33	4.858
	30.76	7.092	3950	16.22	22.56	4.008	0.004	0.067	3.975	4.667
	98.91	14.89	17180	5.483	28.58	5.661	0.017	0.706	7.432	8.782
	827.6	11.42	95520	161.4	12.67	92.38	0.007	5.197	4.142	4.687
576RP-3-B*	819.4	32.23	22610	60.2	35.42	7.804	0.026	1.269	7.295	8.313
576RP-3-C*	250.9	5.524	21220	54.31	6.578	6.195	0.001	1.271	2.189	2.452
	391.5	7.227	30160	77.85	13.83	9.119	0.001	1.763	2.886	3.41
	637.3	9.757	53030	119.2	21.46	14.3	0.002	2.549	3.25	3.671
576RP-5-A*	281.7	9.24	24730	127	11.16	8.267	0.01	2.213	4.516	4.835
	170.2	13.08	17100	86.8	15.36	5.211	0.025	1.133	6.184	10.44
	1284	11.43	92660	360.1	21.4	36.42	0.009	11.07	6.606	6.054
576RP-5-B*	496.1	7.668	30290	149.1	9.26	16.53	0.01	3.199	3.353	3.394
	532.2	11.06	54020	177	18.11	23.33	0	4.772	6.202	6.984
	3449	12.93	228900	809	46.11	68.17	0.003	25.21	5.066	5.287
576RP-5-C*	2480	9.987	210900	734.3	17.56	141.1	0	19.05	3.603	3.344
	1836	9.207	177200	543.7	15.31	138.7	0.012	16.88	3.933	3.982
	2345	13.06	206400	619.7	22.44	129.2	0.005	19.47	6.097	6.784
224RP-3	77.04	12.48	7223	46.57	9.496	2.242	0	0.385	5.241	5.817
	65.93	7.052	4438	36.25	4.059	1.49	0	0.367	3.582	3.086
	166.8	9.668	26370	59.52	8.189	4.428	0	0.491	3.724	3.331
	76.87	10.36	8874	50.79	10.91	2.062	0.003	0.446	4.415	4.778
227RP-7	149.5	39.44	26140	203.5	60.72	37.28	0.067	6.887	42.42	45.47
	131.6	43.15	24060	107.5	433.5	34.53	0.102	6.105	55.8	64.07
	162.6	40.63	26130	181.9	46.14	36.17	0.166	8.059	35.03	41.87
	140.4	25.04	22150	97	41.62	12.73	0.036	5.365	26.64	27.88

Ochre

1031	17.77	3.732	18450†	35.92	67.15	0.636	0.03	4.321	11.75	13.75
Beehive Hill	29.29	8.006		89.88	36.56	1.141	0.064	5.199	56.47	49.56
	38.78	23.31		53.09	30.47	1.652	0.073	6.089	8.968	10.18
	44.52	6.996		104.5	220.2	3.235	0.114	13.37	150.8	166.1
	44.41	11.18		143.7	95.97	1.301	0.124	14.19	36.91	42.09
1035	88.87	30.49	29138	45.01	113.2	1.776	0.141	2.368	33.69	33.53
Beehive Hill	92.10	29.7		46.59	115	4.24	0.085	2.367	168.1	134.6
	88.52	26.12		54.73	102.5	3.634	0.136	3.093	28.51	35.4
	91.77	31.59		39.61	112.5	1.029	0.1	2.435	22.96	23.66
	126.30	37.35		39.21	123.6	0.98	0.18	2.383	28.05	28.72
1036	91.45	30.98	28972	85.8	104.7	1.429	0.085	8.094	31.81	33.79
Beehive Hill	103.40	28.46		102.4	110.6	1.966	0.115	12.14	50.85	63.13
	94.46	30.12		94.55	105.3	1.052	0.098	7.64	35.08	35.06
	92.31	27.54		100.5	103	1.225	0.108	7.838	26.69	29.75
	82.33	33.14		103.2	103.7	1.157	0.19	6.456	24.62	25.72
1037	106.30	46.87	30041	58.9	125.8	1.372	0.146	15.15	82.65	63.54
Beehive Hill	98.10	39.2		58.9	95.08	0.91	0.104	4.842	38.16	33.33
	108.50	36.78		63.23	116.8	1.297	0.118	5.653	25.08	27.97
	99.00	35.13		58.92	92.96	1.31	0.092	6.25	20.61	22.46
	100.40	32.67		59.71	116.6	1.567	0.105	5.717	24.64	28.17

1050 Ragged Top	104.60	108.9	36780	26.11	34.37	1.925	0.19	17.99	15.33	29.24
	102.80	97.19		27.06	30.14	1.971	0.176	18.87	15.07	25.27
	107.50	79.99		40.15	39.03	1.686	0.162	22.43	23.53	33.76
	95.69	101.1		32.22	32.38	2.429	0.164	18.46	23.25	42.89
	103.50	255.3		30.96	48.82	3.252	0.153	18.7	31.49	46.96
1046 Rattlesnake Pass	96.64	121.7	35074	22.42	354.6	4.055	0.11	6.065	12.93	16.13
	94.11	59.7		8.299	110.4	2.566	0.083	6.154	26.34	32.9
	95.66	120.1		25.41	62.4	2.261	0.13	7.054	20.74	24.83
	92.82	112.5		24.33	51.07	4.169	0.099	17.67	23.37	32.31
	79.81	29.69		9.003	44.89	1.101	0.075	3.359	9.37	11.25
1043 Rattlesnake Pass	375.60	61.79	31322	57.84	626.9	5.961	0.226	6.185	134.2	175.6
	119.50	53.87		14.03	103.2	0.946	0.099	2.475	32.13	38.7
	90.49	45.19		15.05	321.8	2.041	0.101	4.384	26.49	48.05
	143.20	59.25		29.69	111.9	1.551	0.087	3.285	29.8	34.32
	116.50	35.23		15.4	124.1	0.968	0.057	3.228	22.55	24.86
1044 Rattlesnake Pass	117.50	30.24	25360	28.98	76.68	1.274	0.052	2.78	28.63	34.21
	91.42	46.17		8.911	50.45	0.693	0.102	3.929	17.74	18.81
	94.53	46.29		16.3	100.7	0.906	0.08	15.85	45.16	48.81
	86.96	38.42		44.03	91.94	0.755	0.063	3.927	74.57	97.77
	100.00	39.04		27.78	115.3	0.781	0.094	4.279	32.56	34.6
1045 Rattlesnake Pass	172.60	72.38	32324	22.39	210.5	4.33	0.162	7.14	26.74	34.29
	101.80	34.24		21.44	65.86	2.727	0.042	2.436	20.34	23.66
	114.70	34.65		8.916	54.35	1.056	0.053	1.446	13.96	14.73
	146.40	28.98		13.9	80.09	1.525	0.067	1.917	21.7	25.07
	122.10	30.16		18.45	80.36	1.669	0.081	2.022	21.34	25.84
1038 Beehive Hill	41.26	16.86	20684	48.01	44.77	0.961	0.045	3.023	14.94	16.9
	41.50	18.09		69.48	133.4	1.598	0.049	3.225	12.81	14.52
	44.13	24.75		46.29	45.3	1.181	0.059	3.302	16.18	19.8
	77.65	152.7		53.56	82.58	4.163	0.065	3.945	10.15	11.26
	55.71	30.08		53.18	43.37	1.549	0.077	3.182	14.67	17.22

Sandstones

SS 2	586.80	120.8	16387	158.9	40.26	9.91	0.071	5.625	25.05	24.19
	699.30	185.3		155.1	34.2	15.96	0.055	5.311	36.42	34.76
	578.00	123.5		135.1	43.33	8.946	0.075	5.5	29.89	27.13
	560.30	133.5		133.4	71.38	10.24	0.091	5.506	25.8	27.3
	561.20	129.5		144.5	46.73	10.05	0.091	6.006	30.23	28.65
SS 3	632.60	82.34	31605	162.6	54.41	5.937	0.126	9.201	20.09	14.42
	631.30	102.8		161.5	69.23	6.38	0.105	8.399	28.45	21.11
	620.50	77.05		155.5	63.34	6.107	0.118	8.395	18.79	14.87
	552.50	63.7		164.9	51.32	6.186	0.102	8.099	15.59	11.47
	609.30	85.19		168.6	57.51	6.576	0.134	8.271	18.37	12.69
SS 5	1136.00	88.21	19855	114.8	164.7	4.397	0.085	7.836	28.14	39.12
	1418.00	119.1		130.1	132.4	6.092	0.085	9.347	34.1	47.73
	912.00	72.7		136.7	102.2	5.038	0.07	9.703	22.24	29.3
	1116.00	85.09		149.4	115.9	5.173	0.079	8.693	24.66	34.07
	1410.00	128.1		150.8	176.7	7.534	0.097	10.52	48.45	61.58

Iron nodule

25.05	0.513	33847	3.361	596.3	2.375	0.119	0.928	138.9	148.9
32.94	0.681		1.015	377	2.015	0.188	1.007	29.75	31.7
11.86	0.346		1.678	581.6	4.396	0.128	0.503	48.24	53.85
34.30	0.39		8.392	408.5	1.977	0.154	1.021	95.96	104.4
27.18	1.009		14.38	363.3	3.146	0.17	1.268	54.17	59.99
32.63	0.193		10.02	804.5	3.049	0.173	1.108	188.5	202.8
25.41	0.803		4.159	786.5	2.965	0.241	1.202	77.24	87.8

* Indicates aliquots where multiple samples were collected from the same spot on the shelter wall.

†The Fe concentrations for ochre, sandstones and iron nodule were measured using XRF.

Appendix 2. Elemental concentrations (ppm) of the pelletized ochre and limonite samples obtained using XRF.

Sample ID	Ti	Mn	Fe	Co	Cu	Zn	As	Pb	Rb	Sr	Zr	Mo	Sb
Ochre 1031	1691	3933	18450	98	0	268	136	59	274	571	161	19	41
Ochre 1035	2728	3946	29138	402	23	126	48	33	260	109	192	12	0
Ochre 1036	2806	6678	28972	275	0	350	141	58	239	160	210	10	0
Ochre 1037	3060	4745	30041	422	32	139	62	40	236	174	308	5	0
Ochre 1038	1619	4595	20684	0	0	168	48	38	214	191	192	23	0
Ochre 1043	4700	1484	31322	283	46	59	17	30	160	1594	247	7	0
Ochre 1044	3426	2416	25360	350	0	74	11	35	140	872	255	7	0
Ochre 1045	5063	2409	32324	421	52	63	21	36	131	2080	217	14	0
Ochre 1046	5021	3560	35074	170	33	80	19	50	163	1059	271	25	0
Ochre 1050	4760	1073	36780	411	0	62	44	22	218	176	224	8	0
sandstone 2	481	0	16387	99	0	69	78	12	23	1398	55	54	0
sandstone 3	992	0	31605	503	49	138	184	18	24	1864	102	24	0
sandstone 5	447	0	19855	363	0	289	102	22	4	3865	104	28	0

Sample		Ochre 1035	Ochre 1035	Paint 75RP-4	Paint 576RP-3-C
		INAA	LA-ICP-MS	(LA-ICP-MS)	(LA-ICP-MS)
V	ave	48.5	97.5	256.5	426.6
	SD	6.0	16.2	194.9	195.6
	% rel SD	12.3	16.6	76.0	45.8
Cr	ave	27.4	31.1	16.9	7.5
	SD	1.4	4.1	1.5	2.1
	% rel SD	4.9	13.1	9.2	28.4
As	ave	38.5	45.0	53.8	83.8
	SD	0.3	6.3	11.8	32.8
	% rel SD	0.7	14.0	21.9	39.2
Zr	ave	34.6	113.4	26.3	14.0
	SD	3.2	7.5	3.0	7.4
	% rel SD	9.3	6.6	11.5	53.3
Sb	ave	2.6	2.5	1.9	1.9
	SD	0.2	0.3	1.0	0.6
	% rel SD	8.2	12.5	53.7	34.6